Transport theory for low-energy positron thermalization and annihilation in helium

G. J. Boyle, M. J. E. Casey, and R. D. White
School of Engineering and Physical Sciences, James Cook University, Townsville, Queensland 4810, Australia

J. Mitroy
School of Engineering, Charles Darwin University, Darwin, Northern Territory 0909, Australia
(Received 20 December 2013; published 28 February 2014)

A transport theory that explicitly incorporates loss of flux due to annihilating collisions is developed and applied to low-energy positron diffusion and annihilation. The use of more complete momentum transfer and annihilation cross sections for helium has resulted in improved descriptions of the time dependence of $\langle Z_{\rm eff}\rangle$ for positrons injected into gaseous helium. Similarly, the variation of $\langle Z_{\rm eff}\rangle$ versus E/n_0 for experiments where the annihilation region is immersed in an electric field is in closer agreement with experimental data. Inclusion of loss of flux due to annihilation was found to have a very small effect on the derived $\langle Z_{\rm eff}(t)\rangle$ for helium.

DOI: 10.1103/PhysRevA.89.022712 PACS number(s): 34.80.Uv, 34.80.Bm, 51.10.+y, 03.65.Nk

I. INTRODUCTION

In the classic positron gas annihilation experiment [1–3], positrons are emitted into a gas, undergo thousands of inelastic collisions while thermalizing, and eventually a mixture of low-energy positrons and ortho-positronium is left in the gas. The free positrons and ortho-positronium then experience elastic collisions until they are in thermal equilibrium with the gas. When positrons collide with atoms, there is always the possibility of in-flight annihilation of the positron with the atomic electrons and experiments typically result in the determination of a number of annihilation parameters. One parameter is the positronium fraction, i.e., the number of positrons surviving in the form of free positronium. Another parameter is the annihilation parameter, $Z_{\rm eff}(v)$, which can be defined in terms of the spin-averaged annihilation cross section, $\sigma_{\rm ann}(v)$, by the identity [4],

$$Z_{\rm eff}(v) = \frac{v\,\sigma_{\rm ann}(v)}{\pi c r_0^2}, \tag{1}$$

where r_0 is the classical electron radius, v is the positron velocity, and c is the speed of light. The annihilation parameter is determined by measuring the intensity of 2γ annihilation as a function of time. Finally, there is the pick-off annihilation rate which is a consequence of annihilating collisions between the positron in long-lived triplet positronium and the electrons in the target atom.

In addition, the time dependence of $\langle Z_{\rm eff}\rangle$ during thermalization contains information about the momentum transfer cross section, the initial energy distribution of the positrons, and the energy dependence of $\langle Z_{\rm eff}\rangle$. The time-dependent behavior of $\langle Z_{\rm eff}\rangle$ for positrons annihilating in the rare gases has been extracted from the annihilation signal [2,5–8]. Experimental information about the energy dependence of the positron-atom momentum transfer and annihilation cross sections can also be obtained by performing experiments in a static electric field [9]. The presence of the electric field leads to the drifting and diffusing positrons having a different energy distribution at equilibrium.

The present work solves the Boltzmann equation to determine the behavior of $\langle Z_{\rm eff}(t)\rangle$ for positrons thermalizing in helium. The simulations are restricted to positrons with an energy below the positronium formation threshold where the only possible processes are elastic scattering and positron annihilation with the atomic electrons. The present solutions gave a fit to the experimental data [2,7] that was significantly improved over previous simulations [7,10]. The variation of the equilibrium $\langle Z_{\rm eff}\rangle$ versus electric field strength has also been determined and again the agreement with experimental data was a significant improvement over previous calculations [9,10].

II. TRANSPORT MODEL

In positron annihilation studies, positrons are released from a source with an unknown distribution of energies well above thermal energies. The positrons then thermalize through energy and momentum exchanging collisions with the background gas, before eventually annihilating. The process is necessarily nonequilibrium and the positron velocity distribution is non-Maxwellian during the thermalization process. For positron annihilation studies conducted in the presence of an applied electric field, the field drives the electrons out of thermal equilibrium, and the steady-state distribution is no longer Maxwellian in nature. The connection between microscopic scattering processes and macroscopic properties including the measured annihilation rates is made under nonequilibrium conditions through Boltzmann's equation [11]. Under spatially homogeneous conditions, the motion of a dilute ensemble of positrons (charge e) moving through a dense background gas of neutral atoms (density n_0) in the presence of an applied electric field $\boldsymbol{E}$ can be described by the linear Boltzmann equation,

$$\frac{\partial \tilde{f}}{\partial t} + \frac{e\boldsymbol{E}}{m}\cdot\frac{\partial \tilde{f}}{\partial \boldsymbol{v}} = -J(\tilde{f}, f_0), \tag{2}$$

where $\tilde{f}(\boldsymbol{v},t)$ is the single-particle positron velocity distribution function, which is a function of velocity $\boldsymbol{v}$ and time t. The collision operator $J(\tilde{f}, f_0)$ takes into account binary interactions between the positrons of mass m and the atoms of mass m_0, where $f_0(\boldsymbol{v}_0)$ denotes the background gas velocity ($\boldsymbol{v}_0$) distribution function, which is assumed to be Maxwellian at the gas temperature T_0. For the regime of interest, the interaction processes determining the macroscopic properties are elastic scattering and annihilation, characterized, respectively,

by a differential elastic cross section $\sigma(v_{\rm cm},\chi)$ (where $v_{\rm cm}$ and χ are the speed and scattering angle in the center-of-mass frame), and the annihilation cross section $\sigma_{\rm ann}(v_{\rm cm})$. The collision operator is then the sum of the respective operators for each process: $J(\tilde{f},f_0) = J_{\rm elast}(\tilde{f},f_0) + J_{\rm ann}(\tilde{f},f_0)$. Integrating Eq. (2) over velocity space results in the normalization condition:

$$\frac{dN}{dt} = -\langle\lambda(t)\rangle N, \tag{3}$$

where $N(t) = \int \tilde{f}(\boldsymbol{v},t)d\boldsymbol{v}$ is the total number of positrons at time t, and $\langle\lambda(t)\rangle$ is the average annihilation rate:

$$\langle\lambda(t)\rangle = \frac{1}{N(t)}\int J_{\rm ann}(\tilde{f}(\boldsymbol{v},t),f_0)d\boldsymbol{v} = \frac{1}{N(t)}\int\left\{\int v_{\rm cm}\sigma_{\rm ann}(v_{\rm cm})f_0(\boldsymbol{v}_0)d\boldsymbol{v}_0\right\}\tilde{f}(\boldsymbol{v},t)d\boldsymbol{v}. \tag{4}$$

Equations (2) and (4) constitute a system of nonlinear equations that must be solved for $\tilde{f}(\boldsymbol{v},t)$. Normalizing the velocity distribution function such that $f(\boldsymbol{v},t) = N(t)^{-1}\tilde{f}(\boldsymbol{v},t)$, results in the kinetic equation,

$$\frac{\partial f}{\partial t} + \langle\lambda\rangle f + \frac{e\boldsymbol{E}}{m}\cdot\frac{\partial f}{\partial \boldsymbol{v}} = -J(f,f_0), \tag{5}$$

where

$$\langle\lambda(t)\rangle = \int\left\{\int v_{\rm cm}\sigma_{\rm ann}(v_{\rm cm})f_0(\boldsymbol{v}_0)d\boldsymbol{v}_0\right\}f(\boldsymbol{v},t)d\boldsymbol{v}. \tag{6}$$

Equations (5) and (6) constitute a system of nonlinear equations that must be solved for $f(\boldsymbol{v},t)$.

Solution of the hierarchy of kinetic equations (5) requires decomposition of $f(\boldsymbol{v})$ in velocity space. The first step in any analysis is typically the representation of the distribution function in terms of the directions of velocity space through an expansion in spherical harmonics [12]:

$$f(\boldsymbol{v},t) = \sum_{l=0}^{\infty}\sum_{m=-l}^{l} f_m^{(l)}(v,t)Y_m^{[l]}(\hat{\boldsymbol{v}}), \tag{7}$$

where $Y_m^{[l]}(\hat{\boldsymbol{v}})$ are spherical harmonics and $\hat{\boldsymbol{v}}$ denotes the angles of $\boldsymbol{v}$. While common practice is to set the upper bound of the l summation to 1 (i.e., the two-term approximation) and consider only $m = 0$ (i.e., a Legendre polynomial expansion), we do not make any such restrictive assumptions in this theory. In best practice, the integer $l_{\rm max}$ is successively incremented until a prescribed accuracy criterion is met, as considered below. This is a multiterm solution of Boltzmann's equation. Combining Eqs. (5) and (7) leads to the following system of coupled partial integro-differential equations for $f_m^{(l)}$:

$$\sum_{l'm'}\langle lm|\frac{\partial}{\partial t} + \langle\lambda\rangle + \frac{e\boldsymbol{E}}{m}\cdot\frac{\partial}{\partial \boldsymbol{c}} + J|l'm'\rangle\, f_{m'}^{(l')} = 0. \tag{8}$$

Expressions for the matrix elements of the streaming operators are given in [12,13]. The collision matrices, e.g., $\langle lm\,|J|\,l'm'\rangle = [J^l_{\rm elast} + J^l_{\rm ann}]\delta_{ll'}\delta_{mm'}$ are all diagonal in l and m, since the collision operators are all scalars.

For positrons in atomic gases, we take advantage of the small mass ratio and utilize the Davydov operator to describe elastic collisions:

$$J^0_{\rm elast}f_0^{(0)} = \frac{m}{m_0v^2}\frac{\partial}{\partial v}\left\{v\nu_m(v)\left[vf_0^{(0)} + \frac{kT_0}{m}\frac{\partial}{\partial v}f_0^{(0)}\right]\right\}, \tag{9}$$

$$J^l_{\rm elast}f_m^{(l)} = \nu_l(v)f_m^{(l)}\delta_{ll'}\delta_{mm'} \quad \text{for} \quad l \geqslant 1, \tag{10}$$

and

$$\nu_l(v) = n_0v2\pi\int_0^{\pi}\sigma(v_{\rm cm},\chi)\,[1 - P_l(\cos\chi)]\sin\chi\,d\chi. \tag{11}$$

We note for $l = 1$, $\nu_1 = \nu_m = n_0v\sigma_{\rm MT}$ is the momentum transfer collision frequency for elastic collisions. In this low mass-ratio limit, the annihilation collision operator takes the form,

$$J^l_{\rm ann}f_m^{(l)} = \nu_{\rm ann}(v)f_m^{(l)}\delta_{ll'}\delta_{mm'} \quad \text{for} \quad l \geqslant 0, \tag{12}$$

where $\nu_{\rm ann} = n_0v\sigma_{\rm ann}(v)$ is the annihilation collision frequency, and hence,

$$\langle\lambda(t)\rangle = 4\pi\int\nu_{\rm ann}(v)f_0^{(0)}(v,t)v^2dv. \tag{13}$$

The annihilation rate can be expressed in terms of the $Z_{\rm eff}(v)$ parameter via

$$Z_{\rm eff}(v) = \frac{1}{\pi r_0^2cn_0}\nu_{\rm ann}(v). \tag{14}$$

Likewise the average of $Z_{\rm eff}(v)$ is related to the average annihilation rate via

$$\langle Z_{\rm eff}(t)\rangle = \frac{1}{\pi r_0^2cn_0}\langle\lambda(t)\rangle. \tag{15}$$

The value of $\langle Z_{\rm eff}(t)\rangle$ when thermal equilibrium is reached for a given gas temperature is denoted as $\langle Z_{\rm eff}\rangle_T$. Another macroscopic variable of interest in the current investigation is the mean energy of the positrons:

$$\langle\varepsilon(t)\rangle = 4\pi\int\frac{1}{2}mv^2f_0^{(0)}(v,t)v^2dv. \tag{16}$$

Details of the numerical solution of the system of equation can be found in [14]. First, it must be emphasized that we do not assume that annihilation can be treated perturbatively [7] (i.e., setting $J_{\rm ann} \approx 0$). The explicit modification of the distribution function due to the annihilation processes is strictly accounted for in a self-consistent manner. Secondly, this is a true multiterm theory, with none of the limitations of the two-term approximation used in previous treatments [7,10]. There are no *a priori* assumptions on the quasi-isotropy of the velocity distribution function. Further, higher-order collision frequencies of Eq. (11) including further angular dependence (i.e., beyond the momentum transfer cross sections) are accurately included in this multiterm theory.

III. COLLISION MODEL

The collision model is based upon an earlier semiempirical model of positron scattering and annihilation [15]. In this model, the interaction between the positron and the atoms was written as the sum of two terms. The first term is the repulsive direct interaction as computed from the Hartree-Fock wave function of the target atom. The second term is a

semiempirical polarization potential. In the earlier work [15], a single polarization potential was used for all partial waves. In the present work, the polarization potential depends on the orbital angular momentum L of the colliding positron. The effective Hamiltonian (in atomic units) for the positron with coordinate $\mathbf{r}_0$ moving in the field of the atom is

$$H = -\tfrac{1}{2}\nabla_0^2 + V_{\rm dir}(\mathbf{r}_0) + V_{\rm pol}^L(\mathbf{r}_0). \tag{17}$$

The polarization potential is given the form,

$$V_{\rm pol}^L(\mathbf{r}_0) = -\frac{\alpha_d\left[1-\exp\left(-r_0^6/\rho_L^6\right)\right]}{2r_0^4}, \tag{18}$$

where α_d is the static dipole polarizability. The adjustable parameter ρ_L is fixed by reference to some external factor, e.g., the value of the scattering length as deduced from a high precision *ab initio* calculation. All the complicated many-body interactions between the positron and atomic electrons can be absorbed into the polarization potential. There have been many investigations of positron-atom interactions in the past that have used conceptually similar Hamiltonians [16–23].

The underlying philosophy of the collision model is semiempirical; no attempt at determining the specific form of the polarization potential by *ab initio* calculation is made. Phase shifts and cross sections produced by this approach have been shown to reproduce *ab initio* calculations over an energy range up to 10 eV provided the adjustable parameter in the polarization potential, namely $\rho_{\rm L}$ is tuned to reproduce the *ab initio* phase shift at some energy [15]. The total elastic $\sigma_{\rm T}$ and momentum transfer $\sigma_{\rm MT}$ cross sections are calculated using formulas from [24], namely,

$$\sigma_{\rm T} = \frac{4\pi}{v^2}\sum_{\ell=0}(2\ell+1)\sin^2(\delta_\ell), \tag{19}$$

$$\sigma_{\rm MT} = \frac{4\pi}{v^2}\sum_{\ell=0}(\ell+1)\sin^2(\delta_{\ell+1}-\delta_\ell), \tag{20}$$

where δ_ℓ are the phase shifts.

Besides reproducing the low-energy elastic cross section, this model potential approach also does a reasonable job of reproducing $Z_{\rm eff}(v)$. The annihilation parameter is computed from the scattering wave function using [4,25,26]

$$Z_{\rm eff}(v) = N_e\int d^3\tau\ \left|\Psi(\mathbf{r}_1,\ldots,\mathbf{r}_N)\Phi(\mathbf{v},\mathbf{r}_N)\right|^2, \tag{21}$$

where $\Psi(\mathbf{r}_1,\ldots,\mathbf{r}_N)$ is the antisymmetrized wave function of the target atom, $\Phi(\mathbf{v},\mathbf{r}_N)$ is the positron scattering function, and $d^3\tau$ represents an integration over all electron coordinates. Equation (21) is not completely general as the total system wave function is assumed to have the product form $\Psi(\mathbf{r}_1,\ldots,\mathbf{r}_N)\Phi(\mathbf{v},\mathbf{r}_0)$. The expression for $Z_{\rm eff}(v)$ given by Eq. (21) is *spin averaged*. In the plane wave Born approximation, where the positron wave function is written as a plane wave, the annihilation parameter is equal to the number of atomic electrons, i.e., $Z_{\rm eff}(v) = N_e$.

The $Z_{\rm eff}(v)$ predicted by Eq. (21) is likely to be an underestimate. The attractive nature of the electron-positron interaction leads to strong electron-positron correlations that increase the electron density at the position of the positron, and consequently enhances the annihilation rate [27–30]. Therefore, an L-dependent enhancement factor G_L is used to rescale the calculated $Z_{\rm eff}(v)$ for a given partial wave by a multiplicative factor G_L, i.e., values for $Z_{\rm eff}^G(v)$ would be computed by

$$Z_{\rm eff}^G(v) = \sum_L Z_{L,\rm eff}^G(v) = \sum_L G_L Z_{L,\rm eff}(v), \tag{22}$$

where $Z_{L,\rm eff}(v)$ is the partial annihilation rate for a positron with angular momentum L scattering from the model potential. The values of G_L are fixed by reference to a high-quality *ab initio* calculation or to experimental data. This work is concerned with low-energy scattering and under these circumstances the relative collision momentum distribution of the annihilating electron-positron pair is not expected to change much as the positron energy changes slightly. This means that the errors in using an energy-independent enhancement factor should not be too large [31,32]. There have been a number of investigations that have shown that a single multiplicative factor (for each L) can adequately represent the magnitude and energy dependence over the energy range below the first excitation threshold [15,33–36].

A. Defining ρ_L and G_L for He

The ability of the model potential calculations to realistically describe the low-energy elastic and annihilation cross sections depends crucially upon the choice of ρ_L and G_L. A number of sources have been used to provide the reference data which was used to fix ρ_L and G_L which are tabulated in Table I. The cross section computed with the values in Table I is termed the model potential (MP) cross-section set.

The value of ρ_0 was almost the same used in [15]. This was set by the requirement that the phase shift at $v = 0.2\ a_0^{-1}$ was the same as that from a Kohn variational calculation from the University College London (UCL) group [38]. We have also used the confined variational method (CVM) [42] to compute the s-wave phase shift at $v = 0.2\ a_0^{-1}$. The CVM phase shift of 0.0406 rad is compatible with the UCL phase shift of 0.041(1) rad [38].

The value of G_0 was set using $Z_{\rm eff}(v=0)$ as calculated with the Kohn variational method [39] using a basis of explicitly correlated Gaussians [43]. This calculation was performed at Charles Darwin University (CDU). The annihilation parameter converges slowly as the basis set increases and one typically finds that $Z_{\rm eff}(v)$ increases as the dimension of the basis increases. The CDU value of $Z_{\rm eff}(v=0)$ is about 2% larger than the Kohn variational value of 3.93 from the UCL group [40]. The CDU value is preferred for two reasons. First, there were absolutely no constraints imposed upon the representation of the helium ground-state wave function. Such constraints are a potential issue with the Kohn calculations from the UCL group [44]. Second, the UCL $Z_{\rm eff}(v=0)$ value comes from an analytic representation of the low-energy $Z_{\rm eff}(v)$ which has an incorrect functional form. The UCL fitting formula contains a term linear in v, but this is not compatible with the effective range expansion for the low-energy $Z_{\rm eff}(v)$ [45]. Moreover, the zero-energy $Z_{\rm eff}$ of 3.99 implies that the room temperature value should be 3.953 and this is compatible with the most precise experimental value of 3.945(20) [2].

TABLE I. The parameters α_d, ρ_L, and G_L for helium in the model potential. The particular numerical criteria (and their source) used to fix ρ_L and G_L are specified.

Atom	α_d (a_0^3)	L	ρ_L (a_0)	Source	G_L	Source
He	1.383 [37]	0	1.510	$\delta_0(v=0.2)=0.041$ [38]	2.979	$Z_{\rm eff}(v=0.0)=3.99$ [39]
		1	1.440	$\delta_1(v=0.3)=0.019$ [38]	3.96	$Z_{\rm eff}(v=0.4)=0.497$ [40]
		2	1.00	$\delta_2(v=0.8)=0.025$ [41]	4.65	He^+ $(G_2-1)/(G_1-1)=1.233$ [36]

The value of ρ_1 was set by reference to the $L=1$ Kohn variational phase shift at $v=0.3\,a_0^{-1}$ [38]. The value of G_1 was set by digitizing the p-wave $Z_{\rm eff}(v)$ taken from Fig. 1 of [38]. The G_1 value of 3.96 is 30% larger than G_0. The tendency for the p-wave enhancement factor to be significantly larger than the s-wave enhancement factor has been noticed for other systems [34–36,46].

The value of ρ_2 was tuned to the $L=2$ phase shift from a convergent close coupling (CCC) calculation [41]. Since there have been no values of $Z_{2,\rm eff}(v)$ published, recourse is made to recent calculations of the He^+ ion [35,36]. The d-wave enhancement factor is 20% larger than the p-wave enhancement factor.

The elastic cross section is depicted in Fig. 1 and compared with other calculations and experiment. Cross sections from a polarized orbital (PO) calculation [26,49] are shown in addition to the calculations mentioned previously. The MP cross section lies very close to the most recent Kohn variational elastic cross section of the UCL group [38]. This was expected since the UCL cross section was used to set the cutoff parameters. The PO calculation gives a scattering length which is larger in magnitude and with a Ramsauer minimum occurring at a higher velocity. The CCC calculation [41] has a scattering length that is slightly smaller in magnitude resulting in a smaller cross section at energies below the Ramsauer minimum. There are two sets of experimental data that are included, those by the Australian National University (ANU) [50] and Kyoto [51]. Cross sections from some older experiments [52,53] are not included to reduce clutter in the figure.

The ANU and Kyoto group elastic cross sections do lie closer to the CCC cross sections at the lowest energies. However, the cross sections based on Kohn variational calculations should be preferred. The Kohn variational phase shifts have been validated by new calculations based on the CVM [39,42] which reproduce the experimental $\langle Z_{\rm eff}\rangle$. The impact of systematic errors in the experiments can become more severe at the lower energies.

Figure 2 plots the momentum transfer cross section as a function of v for energies below the Ps-formation threshold. It is compared with the Kohn variational momentum transfer cross section from the UCL group [38] and the CCC momentum transfer cross section of the Curtin group [41]. The MP cross section lies very close to the momentum transfer cross sections from the UCL and Curtin groups.

The annihilation parameter as a function of v is depicted in Fig. 3. The original $Z_{\rm eff}(v)$ of Campeanu and Humberston [7] is characterized by the small size of $Z_{\rm eff}(v)$ near $v=0.5\,a_0^{-1}$. However, there are some obvious problems with the Campeanu and Humberston $Z_{\rm eff}$. This curve shows a variation of $Z_{\rm eff}(v)$ near $v=0$ that is linear in v. However, an application of effective range theory to annihilating collisions has shown that $Z_{\rm eff}(v)\approx Z_0+v^2Z_2$ where Z_0 and Z_2 are constants [45]. Another limitation of this earlier calculation is the omission of contributions from partial waves with $L>1$. For these reasons the Campeanu and Humberston $Z_{\rm eff}(v)$ should be

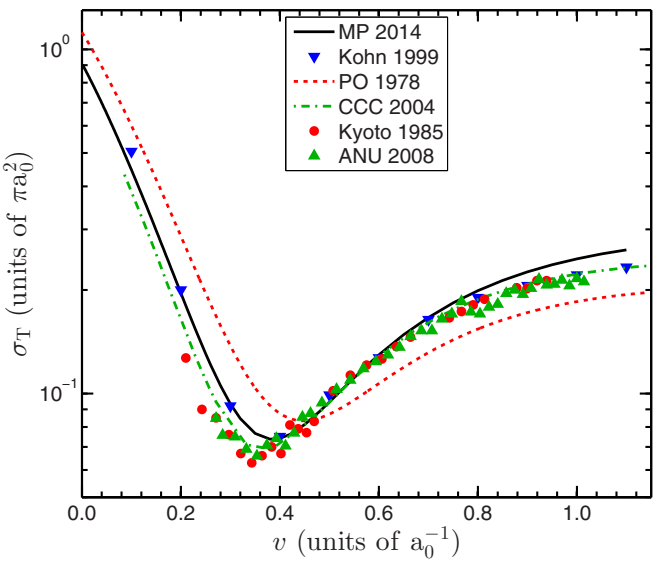

FIG. 1. (Color online) The elastic cross section, $\sigma_T(v)$ (in units of πa_0^2) for positron scattering from helium.

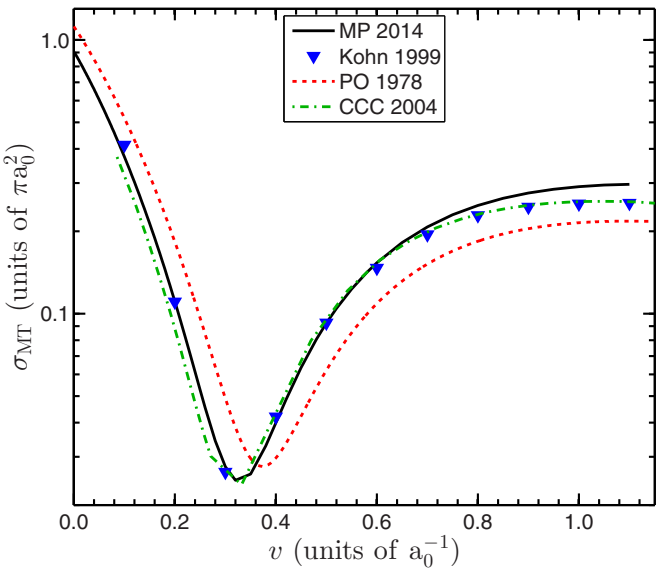

FIG. 2. (Color online) The momentum transfer cross section $\sigma_{MT}(v)$ (in units of πa_0^2) for positron scattering from helium.

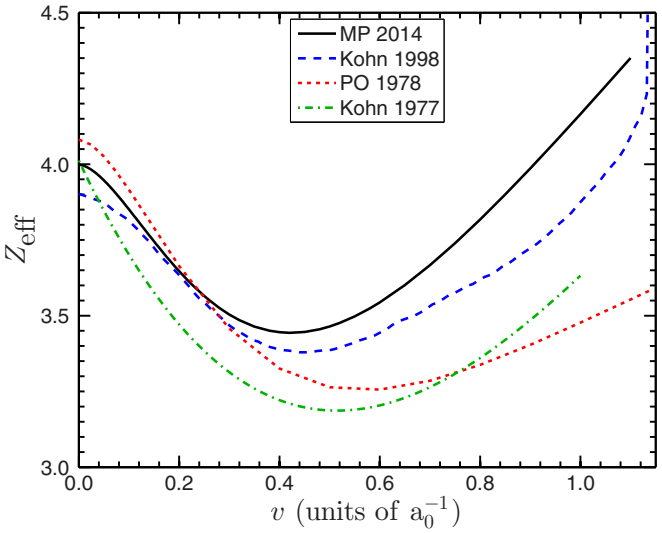

FIG. 3. (Color online) The annihilation parameter $Z_{\rm eff}(v)$ for positron scattering from helium. The 1977 Kohn variational $Z_{\rm eff}(v)$ was taken from Ref. [47] while the 1998 Kohn $Z_{\rm eff}(v)$ was taken from Ref. [48].

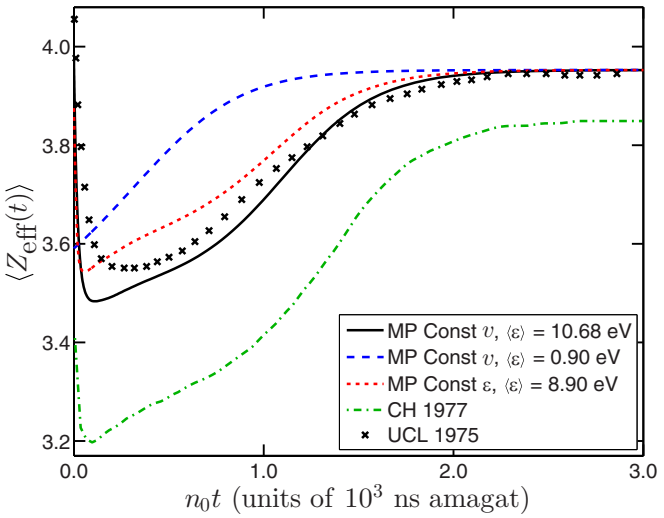

FIG. 4. (Color online) Temporal variation of $\langle Z_{\rm eff}(t)\rangle$ for positrons thermalizing in gaseous helium at a temperature of 293 K. The simulations are compared with the UCL experimental data [2,7] and the CH simulation [7]. The curve representing the UCL experimental $\langle Z_{\rm eff}(t)\rangle$ was taken by digitizing Fig. 3 from [7] with the constraint that the large t asymptote was 3.945 [2]. The different initial distributions are characterized by varying distributions and average energies; Const v is a constant distribution in v space below the Ps threshold; Const ε is a constant distribution in energy space below the Ps threshold. See text for details.

regarded as being superseded by the later Kohn variational calculations [40,48].

The later variational calculation [48] did include contributions from the d wave, and the functional form of $Z_{\rm eff}(v)$ near $v = 0$ is more compatible with the expectations of effective range theory. This later calculation had larger values of $Z_{\rm eff}(v)$ at the minimum despite not including contributions from partial waves with $L > 2$. The MP calculations do include terms from these higher partial waves, with the contribution to $Z_{\rm eff}$ at $v = 1.1\ a_0^{-1}$ being 0.101. This partly explains why the MP $Z_{\rm eff}(v)$ is larger than the Kohn variational $Z_{\rm eff}(v)$.

IV. POSITRON DIFFUSION AND THERMALIZATION CALCULATIONS

A. Positron annihilation in helium under field-free conditions

Initially we consider positron annihilation experiments where positrons are released into a gas of known pressure and the annihilation spectra is measured and interpreted in terms of the transient $\langle Z_{\rm eff}(t)\rangle$ and the steady-state value $\langle Z_{\rm eff}\rangle$. For helium, the experimental results of the UCL group for $\langle Z_{\rm eff}(t)\rangle$ are displayed in Fig. 4 as a function of the reduced time $n_0 t$. Comparison with the calculated transient $\langle Z_{\rm eff}(t)\rangle$ provides some assessment of the positron-helium elastic and annihilation cross sections.

There is limited information regarding the appropriate initial conditions for the speed distribution of the positrons at the start of the $\langle Z_{\rm eff}(t)\rangle$ measurements. Accordingly, there is little point in experimenting with a variety of initial velocity distributions. The initial distributions will have positrons with energies up to the positronium formation threshold. This choice was also made by Campeanu and Humberston [7]. With this choice, there are two obvious distribution functions that can be adopted.

The first of these would be a constant speed distribution, i.e., $f_0^{(0)}(v) = C$ where C is a constant up to some cutoff velocity, $v_{\rm max} = \sqrt{2\varepsilon_{\rm max}/m}$. The mean energy of this distribution function is given by the identity, $\langle\varepsilon\rangle = (3/5)(m v_{\rm max}^2/2)$. For helium, with $v_{\rm max} = 1.1438$ a.u., this leads to $\langle\varepsilon\rangle = 0.39249$ a.u. $=$ 10.68 eV.

The second initial distribution would be one that was constant in energy space, i.e., $f_0^{(0)}(\varepsilon)\varepsilon^{1/2} = C$ where C is a constant up to some cutoff velocity $v_{\rm max}$. The mean energy of this distribution would be $\langle\varepsilon\rangle = (1/2)(m v_{\rm max}^2/2)$. $\langle\varepsilon\rangle =$ 0.32707 a.u. $= 8.90$ eV.

In Figs. 4 and 5 the calculated temporal variation of $\langle Z_{\rm eff}(t)\rangle$ and the mean energy $\langle\varepsilon(t)\rangle$ are plotted. Besides the two distributions specified above, we also show an additional $f_0^{(0)}(v) = C$ distribution with $v_{\rm max} = 0.3320$ a.u. ($\langle\varepsilon\rangle = 0.90$ eV). Also shown in Fig. 4 is the UCL experimental $\langle Z_{\rm eff}(t)\rangle$ and the previous simulation by Campeanu and Humberston (CH) [7]. The UCL $\langle Z_{\rm eff}(t)\rangle$ initially has $\langle Z_{\rm eff}(t = 0)\rangle$ higher than its equilibrium value; it decreases as t increases, until it stabilizes before increasing to its equilibrium (thermal) value. This indicates that the initial velocity distribution should have a mean energy that is larger than the energy where $Z_{\rm eff}(v)$ is smallest. The CH profile, which used a constant speed initial distribution, shows these qualitative features. But, the minimum $\langle Z_{\rm eff}(t)\rangle$ during thermalization is 0.3 smaller than the minimum $\langle Z_{\rm eff}(t)\rangle$ seen for the UCL data and the value after thermalization is achieved is too small by 2.3%.

The $\langle Z_{\rm eff}(t)\rangle$ computed with the MP cross sections are in better agreement with the UCL $\langle Z_{\rm eff}(t)\rangle$. The UCL $\langle Z_{\rm eff}(t)\rangle$ plotted in Fig. 4 were taken from Fig. 3 of [7]. The digitized values were normalized so that the large-t experimental value of $\langle Z_{\rm eff}(t)\rangle$ was 3.945 [2]. The asymptotic value of the MP $\langle Z_{\rm eff}(t)\rangle$ was 3.953. The minimum value of $\langle Z_{\rm eff}(t)\rangle$ is much

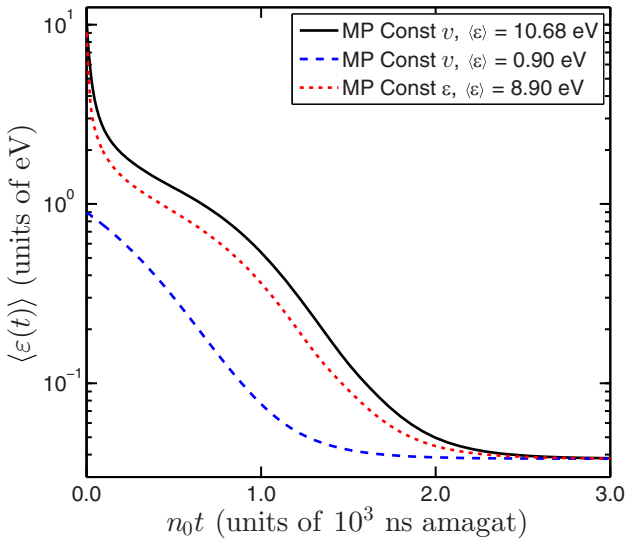

FIG. 5. (Color online) Variation of $\langle\varepsilon(t)\rangle$ for positrons thermalizing in helium for different initial conditions. The temperature of the helium gas was taken as 293 K.

closer to the minimum observed in the UCL experiment. This is a consequence of the larger value of $Z_{\rm eff}(v)$ at the minimum. The thermalization times are also compatible with the thermalization time for the UCL experiment. The initial uniform in speed distribution has a slightly longer thermalization time than the initial uniform in energy distribution.

The very close agreement between the MP and experimental $\langle Z_{\rm eff}\rangle$ has potential implications for the interpretation of the positron lifetime experiment. The conversion factor of $\pi r_0^2 c$ in Eq. (15) comes from a treatment of the positron-electron systems without any quantum electrodynamic (QED) effects and the constant is related to the positronium annihilation rate in the $^1S^e$ state. The inclusion of QED effects decreases the positronium 2γ-annihilation rate by 0.59% [54]. Incorporation of a QED correction into the $\langle\lambda(t)\rangle$ to $\langle Z_{\rm eff}(t)\rangle$ conversion of Fig. 4 would lead to an increase in the experimental $\langle Z_{\rm eff}(t)\rangle$ curve by about 0.024. Even with this shift, the level of agreement between the large-t MP and experimental $\langle Z_{\rm eff}\rangle$ would still be better than 1%.

Both the MP and CH simulations start with $Z_{\rm eff}(v)$ closer to 4.0 at the $v = 0$ threshold. However, the asymptotic value for the CH simulation as $t \to \infty$ is more than 0.1 smaller than experiment and the MP asymptotic values. This is due to the incorrect functional dependence of the CH $Z_{\rm eff}(v)$ with v near $v = 0$. As mentioned earlier, the linear dependence of the CH $Z_{\rm eff}(v)$ with v is incompatible with effective range theory [45].

Figure 4 also depicts $\langle Z_{\rm eff}(t)\rangle$ for a positron distribution with the mean energy located at an energy lower than the minimum in the $Z_{\rm eff}(v)$ profile. The distribution does not show any sign of the minimum in the $\langle Z_{\rm eff}(t)\rangle$ profiles seen in UCL experiment and other simulations.

The transient profiles, including the depth of the minimum, are determined by an interplay between the $\sigma_{\rm MT}(v)$, the annihilation cross section and the initial average energy of the positrons. An initial distribution with positron energies up to the Ps-formation threshold is crucial to giving a correct prediction of the overall thermalization time. While there are small uncertainties in the MP $\sigma_{\rm MT}(v)$, these uncertainties have minimal impacts on the thermalization time and can be effectively neglected as a source of error. The size of the dip in $\langle Z_{\rm eff}(t)\rangle$ is primarily driven by the dip in $Z_{\rm eff}(v)$. The $Z_{\rm eff}(v = 0.42)/\langle Z_{\rm eff}\rangle_T$ ratio is 0.872 for the MP calculation with the $f_0^{(0)}(v) = C$ distribution. The ratio of the dip in $\langle Z_{\rm eff}(t)\rangle$ measured with respect to the $\langle Z_{\rm eff}\rangle_T$ for the UCL data is 0.90. The ratio can be expected to show some sensitivity to the initial positron distribution used to start the simulations.

One characteristic of all the calculated $\langle Z_{\rm eff}(t)\rangle$ in Fig. 4 is shape of the minima which are sharper than the experimental curve. However, the experimental $\langle Z_{\rm eff}(t)\rangle$ was taken with a finite time resolution of 1.92 ns, and subjected to smoothing. A more precise investigation of the effects of time resolution is not possible since Fig. 3 [7] is given in terms of reduced time and the density of the gas was not specified.

B. Positron annihilation in helium in an electric field

The application of an electric field in thermalization experiments drives the positrons out of thermal equilibrium with the background helium gas. The steady state is achieved when the energy gain of the positrons in the electric field is balanced by the energy loss from collisions with helium atoms. The velocity distribution of the positrons in the steady state will no longer be a Maxwellian distribution. As the field strength is increased in magnitude, the cross sections and $Z_{\rm eff}$ are sampled over an increasingly larger energy range. Furthermore, the electric field modifies the steady-state velocity distribution function, and hence $\langle Z_{\rm eff}\rangle$, and necessarily modifies the transient response $\langle Z_{\rm eff}(t)\rangle$. The application of an electric field to the thermalization experiments represents a test on the validity of the cross section set at energies higher than thermal energies.

The variation of the steady-state $\langle Z_{\rm eff}\rangle$ with an applied electric field is displayed in Fig. 6. The MP cross-section

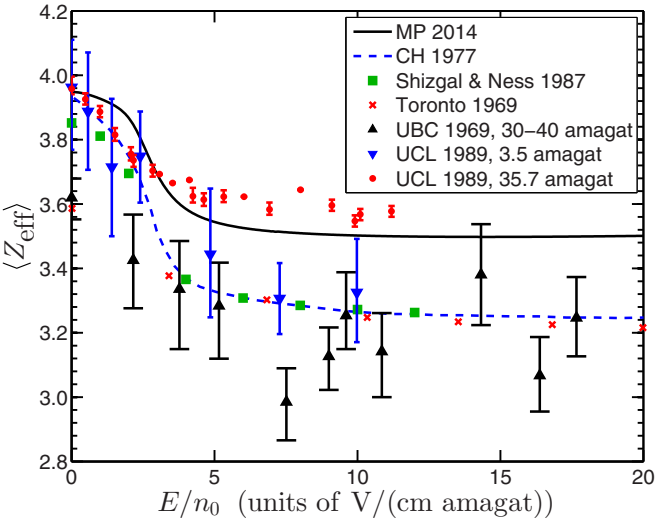

FIG. 6. (Color online) Comparison of steady-state $\langle Z_{\rm eff}(E/n_0)\rangle$ for thermalized positrons in helium at $T_0 = 293$ K. The curve labeled MP 2014 uses the MP cross-section set. Also shown are experiments from the Toronto [5], UBC [55], and UCL [9] laboratories. Previous transport calculations are also depicted [7,10]).

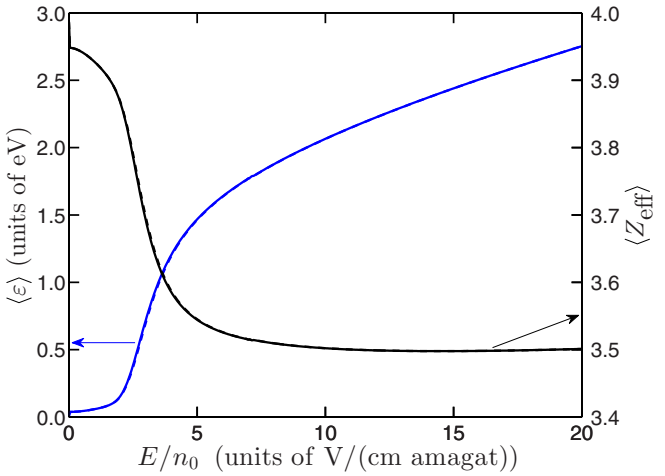

FIG. 7. (Color online) The steady-state $\langle Z_{\rm eff}\rangle$ and mean energy $\langle\varepsilon\rangle$ for positrons thermalizing in helium at $T_0 = 293$ K under the action of a reduced electric field E/n_0 using the new cross-section set.

set is shown as are results from two previous transport calculations [7,10]. Experimental data from the University of Toronto [5], University of British Columbia (UBC) [55], and UCL [9] are presented. All calculated and experimental data show the same trend; there is a tendency for $\langle Z_{\rm eff}(E/n_0)\rangle$ to decrease as the reduced electric field E/n_0 is increased. The reason for the decrease is easily explained by reference to the functional dependence of $Z_{\rm eff}(v)$ and the mean energy of the positron cloud at increasing E/n_0. The increase in mean positron energy with E/n_0 is shown in Fig. 7. The rapid increase in $\langle\varepsilon\rangle$ beginning at 2 V/(cm amagat) is a consequence of the Ramsauer-Townsend minimum in the momentum transfer cross section at around 1.0 eV. For values of $E/n_0 > 5$ V/(cm amagat), the mean energy ranges from 1 to 3 eV where $Z_{\rm eff}(v)$ has a broad minimum with $Z_{\rm eff}(v) \approx 3.5$.

There are effectively four sets of experimental data: the data of the Toronto [5] and UBC [55] experiments, and the two UCL data sets [9] which were taken at densities of 3.5 and 35.7 amagat. The present MP $\langle Z_{\rm eff}(E/n_0)\rangle$ tends to lie higher than three of the experimental data sets. However, two of these data sets (Toronto and UBC) should be given less weight since they do not reproduce the accepted value for the zero-field $\langle Z_{\rm eff}\rangle_T$. The 3.5-amagat data from the UCL experiment have large error bars since the free positron annihilation signal was barely resolvable from the signal due to pick-off annihilation and ortho-Ps decay [9,56]. The most reliable experimental data set would be the 35.7-amagat set from the UCL experiment.

The two previous transport calculations of $\langle Z_{\rm eff}(E/n_0)\rangle$ [7,10] both use roughly the same $Z_{\rm eff}(v)$ and both calculations give $\langle Z_{\rm eff}(E/n_0)\rangle < 3.3$ for $E/n_0 > 5$ V/(cm amagat). The present MP calculations have $\langle Z_{\rm eff}(E/n_0)\rangle \approx 3.5$ for $E/n_0 > 5$ V/(cm amagat). The present MP calculations have a larger $\langle Z_{\rm eff}(E/n_0)\rangle$ simply because the MP $Z_{\rm eff}(v)$ is larger than the CH $Z_{\rm eff}(v)$ for the relevant values of v.

The most significant comparison in Fig. 6 is between the present transport calculation with the MP cross sections and the 35.7-amagat data from the UCL experiment [9]. The UCL data tend to be about 2%–3% smaller than the MP curve for $E/n_0 <$ 3 V/(cm amagat). However, this is a low-energy region where the MP calculation should be most reliable. At these energies, the functional dependence of $Z_{\rm eff}(v)$ is largely governed by effective range theory [45].

At higher electric fields, the MP $\langle Z_{\rm eff}(E/n_0)\rangle$ are larger than the Toronto and UBC data, although generally consistent when the scatter in the data is considered. The MP $\langle Z_{\rm eff}(E/n_0)\rangle$ are, however, slightly below the higher density experimental data of the UCL group [9]. While the higher pressure UCL results [9] are more accurate than their lower pressure results, at 35.7 amagat, these results may include other multiple scattering [57] and density effects [58] which have not been included in our calculations. It is also worth noting that the discrepancy is only 2%–3%.

C. On the accuracy of a perturbation treatment of annihilation and the two-term approximation used in positron transport theory

If the annihilation collision frequency $\nu_{\rm ann}(v)$, or equivalently $Z_{\rm eff}(v)$, increases (decreases) monotonically with energy in the region sampled by the distribution function, there exists a preferential loss of positrons within the higher (lower) energy part of the distribution. The annihilation cross section is usually many orders of magnitude smaller than the momentum transfer cross section and so it is often assumed that annihilation can be treated as a perturbation. The loss of flux due to annihilation is typically omitted during the calculation of the distribution function [i.e., neglect the explicit $\nu_{\rm ann}$ in Eq. (5)].

Calculations of positron transport in helium have also been done with the flux loss due to annihilation included in the calculation of the distribution function. At zero field, this nonperturbative treatment will cause the distribution function to deviate slightly from the expected Maxwellian distribution (at the helium temperature) and therefore result in a small change in the $\langle Z_{\rm eff}\rangle_T$ computed using Eqs. (13) and (15). For helium, the differences between the actual temperature of the thermalized distribution and gas temperature are less than 0.13%, resulting in a change to $\langle Z_{\rm eff}\rangle_T$ of 0.0015%.

The nonperturbative treatment can also be applied to treat the steady-state diffusion of positrons in an electric field. Figure 7 shows the thermalized $\langle Z_{\rm eff}\rangle$ and $\langle\varepsilon\rangle$ for positrons diffusing in an electric field. The differences between the perturbative and nonperturbative treatments are less than 4% for the mean energy and 0.14% for $\langle Z_{\rm eff}\rangle$ over the range $E/n_0 \in [0,20]$ V/(cm amagat). These differences are essentially not visible in Fig. 7.

The validity of the two-term approximation used in earlier transport calculations [7,10] has been checked with an investigation of the impact of the computational parameter $l_{\rm max}$ in the spherical harmonic expansion in Eq. (7). This parameter accounts for the anisotropic nature of the velocity distribution function, and also enables greater account for the anisotropy in the differential cross sections to be included. The parameter $l_{\rm max}$ is incremented until some convergence criteria is met, generally on the macroscopic parameters such as $\langle Z_{\rm eff}\rangle$. It was found that the two-term approximation was sufficient to guarantee accuracy to within 0.01% or better for all transport properties over the range of reduced fields

considered. This is expected since low-energy positron helium elastic scattering is dominated by the *s* wave. Consequently, collisional processes result in large momentum exchanges with small energy exchanges and the quasi-isotropy of the velocity distribution then follows.

V. CONCLUSION

Transport theory calculations of the thermalization and annihilation of positrons diffusing in helium have been completed. The collision cross sections for helium were model potential values that were tuned to the best available calculations and experiments. The present calculations of the positron diffusion are largely compatible with the available experimental information. Lack of detailed knowledge in the energy distributions of the positrons at the start of the simulation does mean that some uncertainty must be attached to any conclusions. The present transport calculations, however, provide a greater degree of consistency with experiment than earlier calculations [10,47]. The closer agreement with the experimental data has largely arisen from a more complete description of the positron-helium annihilation cross section. The use of a two-term distribution function and a perturbative treatment of positron annihilation used in previous studies are found to have a very small effect on the transient and steady-state behavior of the positron cloud.

ACKNOWLEDGMENTS

This work was supported under the Australian Research Council's (ARC) Centre of Excellence program. The authors must thank Professor Igor Bray and Professor Dmitry Fursa for forwarding phase shifts from their CCC calculations for helium.

[1] P. G. Coleman, T. C. Griffith, G. R. Heyland, and T. L. Killeen, J. Phys. B **8**, L185 (1975).
[2] P. G. Coleman, T. C. Griffith, G. R. Heyland, and T. L. Killeen, J. Phys. B **8**, 1734 (1975).
[3] M. Charlton, Rep. Prog. Phys. **48**, 737 (1985).
[4] P. A. Fraser, Adv. At. Mol. Phys. **4**, 63 (1968).
[5] C. Y. Leung and D. A. L. Paul, J. Phys. B **2**, 1278 (1969).
[6] S. J. Tao and T. M. Kelly, Phys. Rev. **185**, 135 (1969).
[7] R. I. Campeanu and J. W. Humberston, J. Phys. B **10**, 239 (1977).
[8] R. I. Câmpeanu, Can. J. Phys. **60**, 615 (1982).
[9] S. A. Davies, M. Charlton, and T. C. Griffith, J. Phys. B **22**, 327 (1989).
[10] B. Shizgal and K. Ness, J. Phys. B **20**, 847 (1987).
[11] L. Boltzmann, Weiner Berichte **66**, 275 (1872).
[12] R. E. Robson and K. F. Ness, Phys. Rev. A **33**, 2068 (1986).
[13] K. F. Ness and R. E. Robson, Phys. Rev. A **34**, 2185 (1986).
[14] R. D. White, R. E. Robson, S. Dujko, P. Nicoletopoulos, and B. Li, J. Phys. D **42**, 194001 (2009).
[15] J. Mitroy and I. A. Ivanov, Phys. Rev. A **65**, 042705 (2002).
[16] V. A. Dzuba, V. V. Flambaum, G. F. Gribakin, and W. A. King, J. Phys. B **29**, 3151 (1996).
[17] H. Nakanishi and D. M. Schrader, Phys. Rev. A **34**, 1810 (1986).
[18] H. Nakanishi and D. M. Schrader, Phys. Rev. A **34**, 1823 (1986).
[19] S.-W. Chiu and D. M. Schrader, Phys. Rev. A **33**, 2339 (1986).
[20] F. A. Gianturco and T. Mukherjee, Nucl. Instrum. Methods Phys. Res., Sect. B **171**, 17 (2000).
[21] J. E. Sienkiewicz and W. E. Baylis, Phys. Rev. A **40**, 3662 (1989).
[22] D. D. Reid and J. M. Wadehra, Phys. Rev. A **50**, 4859 (1994).
[23] L. T. Sin Fai Lam, J. Phys. B **15**, 143 (1982).
[24] R. P. McEachran and A. D. Stauffer, Aust. J. Phys. **50**, 511 (1997).
[25] G. G. Ryzhikh and J. Mitroy, J. Phys. B **33**, 2229 (2000).
[26] R. P. McEachran, D. L. Morgan, A. G. Ryman, and A. D. Stauffer, J. Phys. B **10**, 663 (1977).
[27] J. P. Carbotte and S. Kahana, Phys. Rev. **139**, A213 (1965).
[28] K. G. Lynn, J. R. MacDonald, R. A. Boi, L. C. Feldman, J. D. Gabbe, M. F. Robbins, E. Bonderup, and J. Golovchenko, Phys. Rev. Lett. **38**, 241 (1977).
[29] M. J. Puska and R. M. Nieminen, Rev. Mod. Phys. **66**, 841 (1994).
[30] J. Mitroy and B. Barbiellini, Phys. Rev. B **65**, 235103 (2002).
[31] G. K. Ivanov, Dokl. Akad. Nauk SSSR **291**, 622 (1986) [Dokl. Phys. Chem **291**, 1048 (1986)].
[32] G. F. Gribakin, Phys. Rev. A **61**, 022720 (2000).
[33] J. Mitroy and M. W. J. Bromley, Phys. Rev. A **73**, 052712 (2006).
[34] G. F. Gribakin and J. Ludlow, Phys. Rev. A **70**, 032720 (2004).
[35] S. A. Novikov, M. W. J. Bromley, and J. Mitroy, Phys. Rev. A **69**, 052702 (2004).
[36] D. G. Green and G. F. Gribakin, Phys. Rev. A **88**, 032708 (2013).
[37] J. Mitroy, M. S. Safronova, and C. W. Clark, J. Phys. B **43**, 202001 (2010).
[38] P. Van Reeth and J. W. Humberston, J. Phys. B **32**, 3651 (1999).
[39] J. Y. Zhang and J. Mitroy, Phys. Rev. A **83**, 022711 (2011).
[40] P. Van Reeth, J. W. Humberston, K. J. Iwata, R. J. Greaves, and C. M. Surko, J. Phys. B **29**, L465 (1996).
[41] H. Wu, I. Bray, D. V. Fursa, and A. T. Stelbovics, J. Phys. B **37**, L1 (2004).
[42] J. Y. Zhang, J. Mitroy, and K. Varga, Phys. Rev. A **78**, 042705 (2008).
[43] J. Mitroy, S. Bubin, W. Horiuchi, Y. Suzuki, L. Adamowicz, W. Cencek, K. Szalewicz, J. Komasa, D. Blume, and K. Varga, Rev. Mod. Phys. **85**, 693 (2013).

[44] P. Van Reeth and J. W. Humberston, J. Phys. B **28**, L23 (1995).
[45] J. Mitroy, Phys. Rev. A **66**, 022716 (2002).
[46] J. Mitroy, J. Y. Zhang, M. W. J. Bromley, and S. I. Young, Phys. Rev. A **78**, 012715 (2008).
[47] R. I. Campeanu and J. W. Humberston, J. Phys. B **10**, L153 (1977).
[48] J. W. Humberston and P. Van Reeth, Nucl. Instrum. Methods Phys. Res., Sect. B **143**, 127 (1998).
[49] R. P. McEachran, D. L. Morgan, A. G. Ryman, and A. D. Stauffer, J. Phys. B **11**, 951 (1978).
[50] J. P. Sullivan, C. Makochekanwa, A. Jones, P. Caradonna, and S. J. Buckman, J. Phys. B **41**, 081001 (2008).
[51] T. Mizogawa, Y. Nakayama, T. Kawaratani, and M. Tosaki, Phys. Rev. A **31**, 2171 (1985).
[52] K. F. Canter, P. G. Coleman, T. C. Griffith, and G. R. Heyland, J. Phys. B **6**, L201 (1973).
[53] T. S. Stein, W. E. Kauppila, V. Pol, J. H. Smart, and G. Jesion, Phys. Rev. A **17**, 1600 (1978).
[54] A. Rich, Rev. Mod. Phys. **53**, 127 (1981).
[55] G. F. Lee, P. H. R. Orth, and G. Jones, Phys. Lett. A **28**, 674 (1969).
[56] M. Charlton (unpublished).
[57] Y. Sakai, J. Phys. D **40**, R441 (2007).
[58] I. T. Iakubov and A. G. Khrapak, Rep. Prog. Phys. **45**, 697 (1982).